FTIR spectroscopy and thermodynamics of hydrogen adsorbed in a cross-linked polymer†

Giuseppe Spoto,* Jenny G. Vitillo, Donato Cocina, Alessandro Damin, Francesca Bonino and Adriano Zecchina

Received 19th March 2007, Accepted 20th June 2007
First published as an Advance Article on the web 12th July 2007
DOI: 10.1039/b704041e

The adsorption of H_2 in a cross-linked poly(styrene-*co*-divinylbenzene) (St-DVB) microporous polymer (BET surface area 920 $m^2\ g^{-1}$) is studied by volumetric and gravimetric methods, FTIR spectroscopy at variable temperature (300–14 K) and *ab initio* calculations. At 77 K the polymer reversibly stores up to 1.3 mass% H_2 at a pressure of 1 bar and 1.8 mass% at 10 bar. The adsorption process involves the specific interaction of H_2 with the structural phenyl rings through weak dispersive forces. The interacting molecules become IR active and give rise to vibrational and rotational–vibrational manifestations which are affected by the temperature, the contact time and the H_2 equilibrium pressure. The spectra of the H_2/St-DVB system reported here represent the first IR evidence of the adsorption of hydrogen on unsaturated molecules. The adsorption enthalpy is evaluated by the VTIR (variable temperature IR spectroscopy) method (C. Otero Areán *et al.*, *Phys. Chem. Chem. Phys.*, 2007, DOI: 10.1039/b615535a) and compared with the results of *ab initio* calculations for the H_2/benzene interaction and with literature data.

Introduction

Singling out of safe and efficient storage methods still represents an open problem which needs to be solved in view of the widespread use of hydrogen as energetic vector. Among the envisaged technologies[1–4] reversible adsorption on microporous solids is in principle simple and inexpensive, but yet inadequate to meet the stringent DOE (US Department of Energy) targets for on board hydrogen storage systems (4.5 mass% H_2 by 2007, 6 mass% by 2010 and 9 mass% by 2015). The method is based on dispersive interaction of the H_2 molecule with the surface of the adsorbent and its effectiveness depends essentially on two factors: (i) the energetic of the interaction, which influences the optimal storage temperature,[5] and (ii) the extension of the surface, which relates to the amount of stored gas.[2] Concerning point (i) it has been predicted[5] that enthalpy changes of the order of 15 kJ mol^{-1} are desirable for optimum H_2 storage and delivery at room temperature; for changes of the order of 6 kJ mol^{-1}, as for most carbons, the optimum storage temperature decreases to *ca.* 115 K. On specific adsorption centres, *i.e.* metal ions, the adsorption energy can dramatically increase (for instance, up to *ca.* 70 kJ mol^{-1} for Cu^I),[6] but at the expense of a dramatic decrease of the H_2 gravimetric density.

As far as the effect of the surface area is concerned, the maximum hydrogen uptake attainable by physisorption at affordable temperature (77 K or higher) cannot exceed the monolayer:[2] in this condition the maximum amount of H_2 which can be stored is related to the surface area as 2.27×10^{-3} mass% m^{-2} g; for a solid with BET surface are of *ca.* 1300 $m^2\ g^{-1}$ (as in the case of graphene), the maximum adsorption capacity is then *ca.* 3 H_2 mass%.

It is worth underlining for the scope of this paper that whatever the nature of the adsorbent, the specific surface area can easily be measured by standard volumetric methods (BET). On the contrary, the evaluation of the gas–solid interaction energy by standard calorimetric methods can become troublesome when dealing with values lower than 10–15 kJ mol^{-1}. In this case variable-temperature infrared measurements, while allowing direct estimation of the site-specific adsorption enthalpy, can represent a valid alternative.[7–9]

Different classes of materials have been investigated as possible hydrogen adsorbents. These include carbon in a variety of forms (nanotubes, graphite and graphite nanofibers, activated carbons),[10–16] zeolites and zeotypes,[6,8,17–20] and metal–organic frameworks (MOFs).[21–26] A recent entry is represented by microporous organic polymers.[27–31] Microporous polymers are worthy of attention because, as outlined by McKeown and co-workers,[28] they combine the possibility offered by organic-based structures to engineer the internal voids (providing, for instance, beneficial ultramicro-porosity)[24,32,33] with the advantages deriving from their low intrinsic density (as they are composed of light elements like C, H, O, N), chemical homogeneity, chemical and thermal stability, synthetic reproducibility and affordable production costs. Microporous polymers investigated up to date belong among the (i) hypercross-linked polymers (HCPs)[30,34,35] and (ii) polymers of intrinsic microporosity (PIMs).[36,37] In HCPs the porosity is induced by extensive cross-linking between the

Dipartimento di Chimica IFM and NIS Centre of Excellence of the Turin University, Via Giuria 7, I-10125 Torino, Italy. E-mail: giuseppe.spoto@unito.it; Fax: +39 0116707855; Tel: +39 0116707832

† Part of the *PCCP* series of themed issues on Alternative Fuel Technologies, published in issues 12, 15 and 21 of *PCCP*, 2007.

polymeric chains, which prevent close packing to form a dense, non-permeable structure. This allows preparation of materials with surface areas as high as 2000–2100 $m^2\ g^{-1}$ with interesting properties as adsorbents.[35] It has been, in fact, reported that polystyrene-based HCPs characterized by BET surface area of *ca.* 1470 $m^2\ g^{-1}$ adsorb up to 1.3 mass% H_2 at 77 K and 1 bar and 2.75 mass% at 10 bar;[30] on samples with 1930 $m^2\ g^{-1}$ of surface area the H_2 uptake at 1.2 bar was only slightly higher (1.55 mass%).[31] While these values are still low as compared to the DOE's standards, it is believed that the introduction of specific molecular sorption sites could represent the winning strategy in view of enhancing the performances.[30]

Porosity in PIMs is intrinsic, in the sense that is a consequence of their composition based on large fused-ring subunits (like porphyrin in Porph-PIM or triptycene in Trip-PIM)[28] connected to form open networks. The H_2 uptake by Trip-PIM resulted 2.7 H_2 wt% at 77 K and 10 bar, *i.e.* comparable to that of HCPs, notwithstanding the lower surface area (1050 $m^2\ g^{-1}$).[29] Also for PIMs it is envisaged that new synthetic and post-processing strategies could result in more satisfactory hydrogen uptakes.[28]

Despite the interest aroused by microporous polymers as possible hydrogen storage media, the basic mechanism of interaction of the H_2 molecules with the polymer surface is not known. Also scarce is the knowledge of the adsorption's thermodynamics, the only available data being due to Germain *et al.* who have measured the H_2 adsorption heat on some HCPs from the volumetric isotherms at 77.3 and 87.2 K.[31]

As extensively demonstrated in the literature,[8,9,19,20,25,38,39] the investigation of hydrogen adsorption by FTIR spectroscopy at temperature variable in the 300–14 K range can be helpful in both the above respects. We have therefore decided to investigate by this technique the H_2 adsorption on some commercial resins which can be assumed as model systems representative of HCPs or PIMs. In this paper we report the results obtained for a medium-high surface area (*ca.* 1000 $m^2\ g^{-1}$) poly(styrene-*co*-divinylbenzene) cross-linked polymer (St-DVB), which has been first characterized from the point of view of the textural and adsorptive properties. The spectroscopic data have been validated by *ab initio* calculations, where the H_2/benzene system has been used to simulate the H_2/phenyl interaction revealed by IR spectroscopy. In the next study the scope will be extended to polymers containing elements other than C and H, as is the case of PIMs.

Experimental

The cross-linked polymer used in these experiments was a poly(styrene-*co*-divinylbenzene) resin (hereafter St-DVB) commercialized by Aldrich in form of 300–800 μm beads.

Surface area, pore volume and pore size distribution were obtained by N_2 adsorption measurements carried out at 77 K on a Micromeritics ASAP 2020 sorption analyzer. H_2 adsorption isotherms at 77 K were obtained over the 0–1 bar pressure range by volumetric analysis (on a Micromeritics ASAP 2010C) and over the 0–10 bar by gravimetric methods (on an IGA-002 microbalance supplied by Hiden Analytical Ltd, UK). In both cases, ultra-pure 6.0 grade H_2 (99.9999%V; SIAD) was used, further purified before adsorption on St-DVB by flushing through an All-pure (Alltech) cartridge and through a cold trap maintained at the liquid nitrogen temperature.

St-DVB samples suitable for transmission infrared experiments were obtained by finely grinding the beads in an agate mortar and by pressing the obtained powder in form of thin self-supporting wafers. Before H_2 adsorption the wafer was outgassed overnight under high vacuum (residual pressure $<10^{-6}$ mbar) at 373 K to remove adsorbed impurities. This thermal treatment was performed in the same cryogenic cell (a closed circuit liquid helium Oxford CCC 1204 cryostat properly modified as described elsewhere)[40] allowing the infrared investigation of species adsorbed in controlled temperature (between 300 and 14 K) and pressure (between 0 and 0.5 bar) conditions. IR experiments consisted of three steps. In the first step H_2 (typically 30 mbar) was dosed at 300 K and spectral series recorded upon gradually decreasing the temperature down to 14 K while simultaneously monitoring the gas phase equilibrium pressure. Besides giving information on the nature of the adsorbed species, this procedure also allowed the evaluation of the site-specific adsorption enthalpy.[7–9] In the second step spectra were recorded at fixed time intervals while keeping constant the temperature (14 K) and the equilibrium pressure of the H_2/St-DVB system; this procedure allowed to investigate the change in composition of the adsorbed phase in terms of *ortho*- and *para*-H_2. In the last step the H_2/St-DVB system was progressively outgassed at constant temperature (14 K) to investigate the dependence of the spectral features on the equilibrium gas pressure.

The infrared spectra were recorded on a Bruker Equinox 55 FTIR spectrometer (equipped with an MCT cryogenic detector) with the sample compartment modified to accommodate the cryogenic head; 512 interferograms (recorded at 1 cm^{-1} resolution) were typically averaged for each spectrum.

The Raman spectra of gaseous H_2 (at 4 bar pressure) were recorded on a Renishaw InVia Raman Microscope equipped with a SpectraPhysics Ar+ 514 nm laser source operated at a power of about 8 mW.

Calculations concerning the interaction of H_2 with the benzene ring were performed at the MP2 level in the frozen-core approximation[41] by means of the GAUSSIAN 03 software package.[42] The used basis set was the aug-cc-pVDZ.[43,44] Symmetry constrained optimization of the H_2/C_6H_6 geometry was carried out using the Berny algorithm with analytical gradient. The thresholds for the maximum and the rms forces were set at 0.000015 and 0.000010 a.u., respectively, and those for the atomic displacements at 0.000060 (maximum) and 0.000040 (rms) a.u. The binding energy was corrected for the basis set superposition error (BSSE), following the *a posteriori* method proposed by Boys and Bernardi;[45] the BSSE corrected binding energy (BE^c) was obtained from the computed value (BE) following the equation $BE^c = BE - BSSE$. As BSSE can greatly influence the geometry of the H_2/C_2H_6 complexes, a BSSE-corrected scan of potential energy (PES) was performed. Each point of the PES curve was actually obtained by freely relaxing the H_2/C_6H_6 intramolecular bonds at increasing H_2–C_6H_6 distances. The H–H bond length at the minimum intermolecular distance was then determined

following a further BSSE-corrected potential energy scan. The anharmonic frequency of the ν(HH) mode of H_2 was calculated by the following procedure: (i) the H–H stretching mode was assumed to be not coupled with any other vibration of the H_2/C_6H_6 adduct; (ii) the H–H distance was varied around the equilibrium value (between −0.2 and +0.3 Å in steps of 0.02 Å) and the total BSSE-corrected energy computed at each step; (iii) the computed points were fitted by a sixth degree polynomial (root-mean-square error less than 10^{-6} E_a) and the 1 D nuclear Schrödinger equation solved following the algorithm proposed by Lindberg[46] and coded in the ANHARM program.[47] This procedure allowed to calculate the fundamental (ω_{01}) and the first-harmonic (ω_{02}) frequencies and to evaluate the anharmonic constant (x_e) and the ν(HH) harmonic frequency (ω_e) of adsorbed H_2 following the equations $\omega_0 x_0 = (2\omega_{01} - \omega_{02})/2$ and $\omega_0 = \omega_{01} + 2\omega_0 x_0$. To check for the accuracy, the harmonic stretching frequency of the isolated H_2 molecule was compared to that from a full analytical calculation performed with GAUSSIAN 03: the agreement was within 40 cm^{-1}.

Results and discussion

Textural and adsorptive properties of St-DVB

The N_2 adsorption and desorption isotherms obtained at 77 K for St-DVB are reported in Fig. 1. The adsorption isotherm shows the typical Type I form (following the IUPAC classification) expected for a microporous material.[48] The calculated BET surface area results to be 920 m^2 g^{-1}, *i.e.* intermediate between that of most polymers of intrinsic porosity (PIMs) and of microporous hypercross-linked polymers (HCPs).[28–30] The micropores volume, as obtained by *t*-plot (Harkins and Jura universal thickness curve), is 0.38 cm^3 g^{-1} and represents a relatively large fraction (*ca.* 70%) of the total accessible volume (0.54 cm^3 g^{-1}, calculated as volume of the liquid at $p/p_0 \approx 0.93$).

The pore diameter and the pore size distribution were evaluated using the DFT (density functional theory) method on the basis of the cylindrical pore model proposed by Jaroniec *et al.*[49] (regularization set to 0.10000). As can be observed in Fig. 2, St-DVB has a broad pore size distribution covering the 4–50 Å range, centered at about 16 Å and showing a relatively large fraction of pores in the 4–15 Å range.

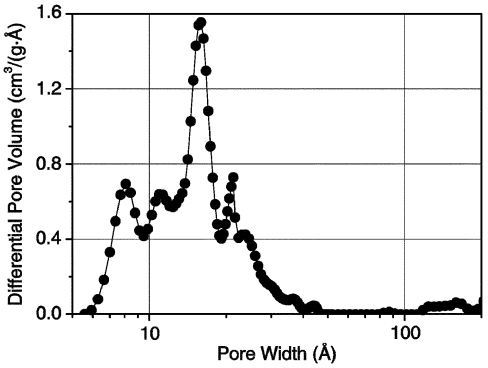

Fig. 2 Differential pore volume for St-DVB calculated using the Tarazona DFT method.

The hydrogen uptake of St-DVB was measured at 77 K *via* volumetric (in the 0–1 bar pressure range) and gravimetric (0–10 bar pressure range) methods: the experimental isotherms are, respectively, reported in Fig. 3 and Fig. 4. It is immediately seen that at 77 K St-DVB can reversibly adsorb up to *ca.* 1.3 H_2 mass% at 1 bar and 1.8 mass% at 10 bar, in good agreement with other microporous polymers of similar textural properties.[28–30]

IR spectroscopy of H_2 adsorbed on St-DVB

Before going to illustrate and discuss the manifestations of H_2 adsorbed on St-DVB, it is useful for the sake of clarity to shortly summarize the basic spectroscopic properties of the dihydrogen molecule in the free (gaseous) state. These are dictated by the facts that:[50] (i) hydrogen molecules exist as two isomers differing for the orientation of the nuclear spins, *i.e.* *para*- (nuclear singlet state, $I = 0$) and *ortho*-H_2 (nuclear triplet state, $I = 1$); (ii) nuclear statistics confines the two spin isomers to different rotational states, those characterized by even J (rotational quantum number) values for *para*- and by odd J values for *ortho*-H_2.

The two isomers give rise to distinguishable spectroscopic manifestations in the Raman spectrum of normal H_2, which is reported in Fig. 5 in the rotational (300–900 cm^{-1}), vibrational

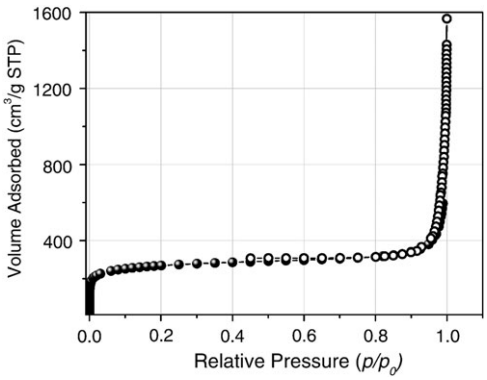

Fig. 1 N_2 adsorption (filled symbols) and desorption (open symbols) isotherms at 77 K for St-DVB.

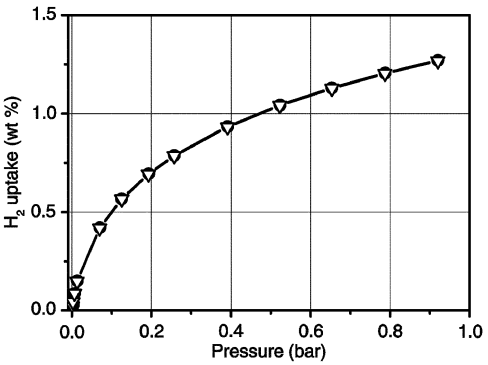

Fig. 3 Volumetric H_2/St-DVB adsorption isotherms recorded at 77 K: first (circles) and second (triangles) isotherms.

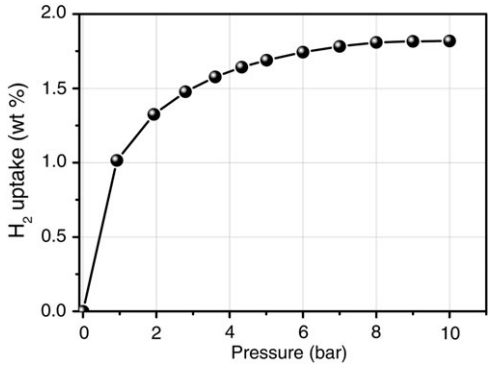

Fig. 4 Gravimetric H_2/St-DVB adsorption isotherm recorded at 77 K.

(4100–4220 cm^{-1}) and rotational–vibrational (4750–4450 cm^{-1}) regions.

More in detail, in Fig. 5 (where the peaks are labelled following the usual spectroscopic nomenclature):

(i) the $S_0(0)$ band at 355 and the $S_0(1)$ at 587 cm^{-1} are due to the rotational transitions $J = 0 \rightarrow J = 2$ of *para*- and $J = 1 \rightarrow J = 3$ of *ortho*-H_2 species, respectively; the 1 : 3 intensity ratio reflects the relative natural abundance of the *para* and *ortho* spin isomers; the $S_0(2)$ component at 817 cm^{-1} is due to the $J = 2 \rightarrow J = 4$ transition of the *para* isomer.

(ii) The Q-type bands at 4161, 4155, 4143 and 4126 cm^{-1} are all due to pure H–H vibrational transitions satisfying the $\Delta v = 1$ and $\Delta J = 0$ selection rule; their assignment is as follows. The bands at 4161, $Q_1(0)$, and 4143 cm^{-1}, $Q_1(2)$, are originated by *para*-H_2 molecules, respectively occupying the $J = 0$ and the $J = 2$ rotational levels of the ground vibrational state; those at 4155, $Q_1(1)$, and 4126 cm^{-1}, $Q_1(3)$, by *ortho*-H_2 molecules in the $J = 1$ and $J = 3$ states.[51,52] It is noteworthy (see Table 1) that the $Q_1(0)$ and $Q_1(1)$ components shift to lower frequency (8–12 cm^{-1}) on passing from gaseous to liquid and solid H_2 (the $Q_1(2)$ and $Q_1(3)$ components being not observed in condensed phases because of the depopulation of the involved rotational levels) and their separation increases, passing from

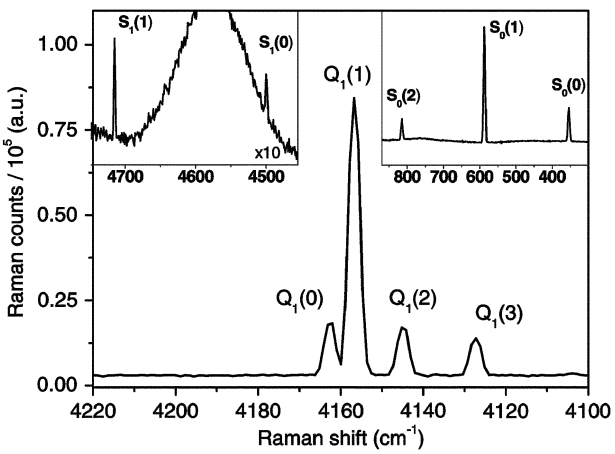

Fig. 5 Rotational (300–900 cm^{-1} region), vibrational (4100–4200 cm^{-1} region) and rotational–vibrational (4450–4750 cm^{-1}) Raman spectrum of gaseous H_2. The intense broad band at *ca.* 4570 cm^{-1} is due to fluorescence by the quartz cell.

Table 1 Vibrational, $Q_1(J)$, and rotational–vibrational, $S_1(J)$, frequencies (in cm^{-1}) of hydrogen in the free state (gas, liquid and solid phases)[51,52,55] and adsorbed on St-DVB [this work]

	Gas	Liquid	Solid	Adsorbed
$Q_1(0)$	4161	4154	4152	4126 (35)[a]
$Q_1(1)$	4155	4146	4143	4112–4118 (43–37)[a]
$Q_1(2)$	4143	—	—	—
$Q_1(3)$	4126	—	—	—
$S_1(0)$	4500	—		4445 (55)[a]
$S_1(1)$	4715	—		4680–4694 (35–21)[a]

[a] Downward frequency shift with respect to gaseous H_2 (in modulus).

6 (gas) to 9 (solid) cm^{-1}. The spectrum of gaseous H_2 also shows vibrational–rotational components in the 4750–4450 cm^{-1} region (inset in Fig. 5): the lower in frequency is the $S_1(0)$ at 4500 cm^{-1} originated by the $v = 0 \rightarrow v = 1$ and $J = 0 \rightarrow J = 2$ transition of *para*-H_2; the next one is the $S_1(1)$ ($v = 0 \rightarrow v = 1$ and $J = 1 \rightarrow J = 3$) at 4715 cm^{-1} due to *ortho*-H_2. In conclusion of this summary of the H_2 spectroscopic properties, it is worth recalling that interconversion of *ortho*-H_2 to the more stable *para* form is very slow even in the liquid state,[53] since it requires asymmetrical change of the nuclear spins. However interconversion can be promoted by spin catalysis (*vide*, for instance, ref. 54 and references therein) following adsorption on solids providing a highly magnetic surface or capable of H_2 dissociation and recombination.

The spectra of H_2 adsorbed on St-DVB, are collected in Fig. 6. They show absorptions in the whole 4750–4100 cm^{-1} interval which are affected by (i) the sample temperature (curves 1–7 in Fig. 6a), (ii) the contact time (curves 8–12 in Fig. 6a) and (iii) the H_2 equilibrium pressure (curves 13–22 in Fig. 6b). For the sake of clarity, in the following these effects will be described and discussed separately.

Considering the effect of the gradual lowering of the temperature, it can be observed in Fig. 6a that cooling the St-DVB sample in H_2 atmosphere results in the appearance of a couple of bands at 4112 and *ca.* 4680 cm^{-1} (together with a much weaker and broad absorption at *ca.* 4445 cm^{-1}) as soon as the temperature reaches 95 K (curve 2 in Fig. 6a). Upon further decreasing the temperature down to 14 K (curves 3–7 in Fig. 6a) the 4112 and 4680 cm^{-1} doublet grows in intensity while shifting to higher frequency (being finally observed at 4118 and 4694 cm^{-1}). On the basis of the data concerning free H_2 in Table 1 and by comparison with the spectroscopy of H_2 adsorbed at the internal surface of inorganic[19,20,56] and metallorganic[25] microporous materials (as well as at the external surfaces of bulky oxidic systems)[39] the assignment of the above manifestations to the ν(HH) stretching mode (Q-type band at 4112–4118 cm^{-1}) and to rotational–vibrational transitions (S-type bands at 4680–4694 and 4445 cm^{-1}) of H_2 molecules polarized (and hence IR activated) by the St-DVB surface is straightforward. In more detail, we assign the 4112–4118 and the 4680–4694 cm^{-1} manifestations to the $Q_1(1)$ and $S_1(1)$ transitions, respectively, of adsorbed *ortho*-H_2 and the very weak component at 4445 cm^{-1} to the $S_1(0)$ mode of the less abundant *para*-H_2 species (see Table 1). The corresponding $Q_1(0)$ mode is expected to be downward-shifted of *ca.* 353 cm^{-1} (pure rotational frequency) or less (because of anharmonicity and non-rigidity effects), *i.e.* in a region where

it is possibly obscured by the much stronger $Q_1(1)$ band. That this is actually the case will be clear in the following, when discussing the effect of the contact time. It is worth underlining that the presence, even at 14 K, of the $S_1(0)$ and $S_1(1)$ rotational–vibrational absorptions is a clear indication that the adsorbed species still possess rotational degrees of freedom, so suggesting that the H_2/St-DVB interaction is of very weak nature. The validity of this conclusion will be demonstrated by the evaluation of the adsorption enthalpy from the spectral series at variable temperature, as described in the next section.

As far as the effect of the contact time at constant temperature (14 K) on the spectroscopic manifestations of the H_2/St-DVB system is concerned, it is evident in Fig. 6a (spectra 8–12) that the $S_1(1)$ rotational–vibrational component is progressively reduced in intensity with the parallel intensification of the $S_1(0)$ one: this represents the direct evidence of the change in composition of the adsorbed H_2 phase which becomes progressively enriched by *para*-H_2 at the expense of the (adsorbed) *ortho* isomer. This conclusion is further supported by the parallel changes occurring in the 4000–4200 cm^{-1} region. It can, in fact. be observed in Fig. 6a that the intensity of the $Q_1(1)$ vibrational manifestation of *ortho*-H_2 at 4118 cm^{-1} decreases with time (as the $S_1(1)$ counterpart), finally becoming a shoulder of a new absorption at 4128 cm^{-1} grown in parallel with the $S_1(0)$ component. The latter absorption can be safely assigned to the $Q_1(0)$ manifestation of adsorbed *para*-H_2 molecules. Although more experimental work is needed to establish whether the *para*-H_2 enrichment is related to some direct catalytic effect exerted by the St-DVB substrate (speeding up the *ortho–para* conversion process in the adsorbed phase) or has different origin, the potentialities of the spectroscopic method in giving a very detailed description of the whole adsorption process are evident.

H_2 adsorption on St-DVB is fully reversible at 14 K, as demonstrated by the fact that all the manifestations described above disappear upon decreasing the H_2 equilibrium pressure (Fig. 6b). It is worth noting that the $Q_1(0)$ band gradually shifts from 4126 to 4114 cm^{-1} and the $S_1(0)$ from 4449 to 4435 cm^{-1} upon outgassing: similar effects have already been observed for H_2 adsorbed in other microporous systems like zeolites and related to the lateral interaction between the molecules in the adsorbed layer.[39] It is conceivable that for St-DVB the shift is more related to the heterogeneity of the systems in terms of pores distribution (as evident from Fig. 2). This means that the component at 4114 cm^{-1} could be associated to the more strongly perturbed H_2 molecules first filling the smallest cavities, and the apparent shift at higher frequency to progressive filling of larger pores by less perturbed molecules. As will be better discussed in the following, the IR manifestations in Fig. 6 can be assigned to the specific adsorption of H_2 on the electron-rich part of the St-DVB structure, *e.g.*, the phenyl rings. The spectra of Fig. 6 then represent the first spectroscopic evidence of the adsorption of molecular hydrogen on unsaturated organic molecules.

Theoretical investigation of the H_2/St-DVB interaction

The possibility of interaction of the H_2 molecule with the delocalized electronic cloud of aromatic systems has been advanced in the past to account for hydrogen adsorption on graphitic carbons[16] and already investigated by theoretical methods.[57–60] In particular, it has been predicted that the

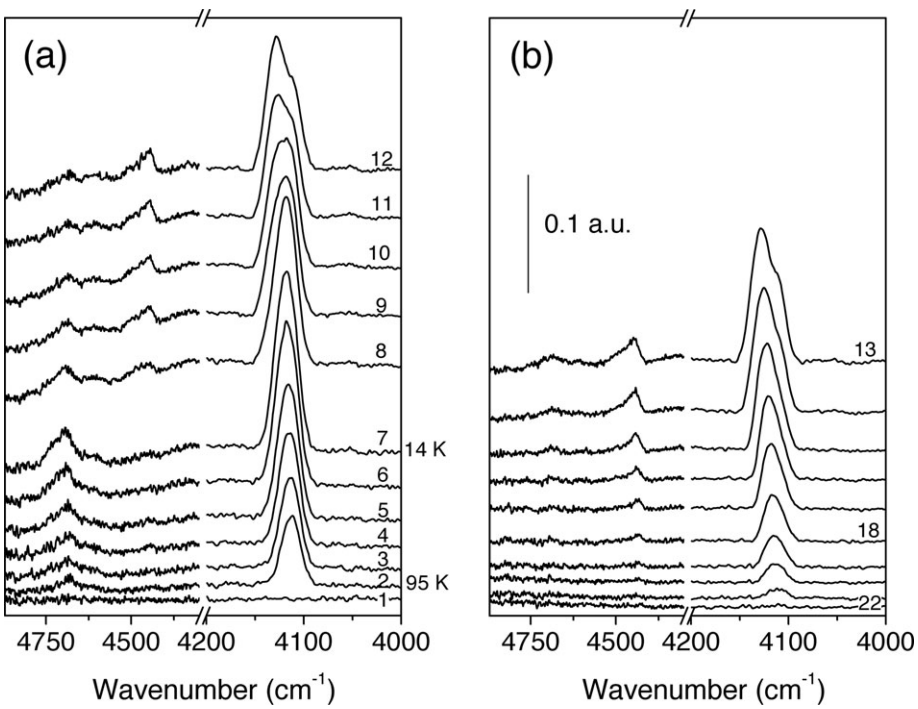

Fig. 6 Infrared spectra of H_2 adsorbed (30 mbar at 300 K) on St-DVB as a function of (i) the temperature in the 100–14 K interval (part a, spectra 1–7); (ii) the contact time at 14 K in the range 0–12 h (part a, spectra 8–12) and (iii) the equilibrium gas pressure at 14 K in the range 12–0 mbar (part b, spectra 13–22).

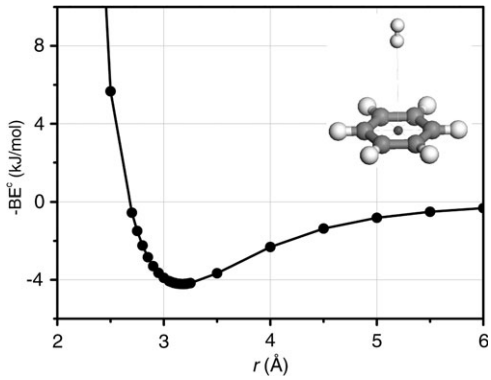

Fig. 7 PES curve for the H_2/C_6H_6 complex in the end-on configuration. Calculated energies for increasing r values (where r is the distance between the centers of mass of the H_2 and C_6H_6 molecules) at MP2/aug-cc-pVDZ level.

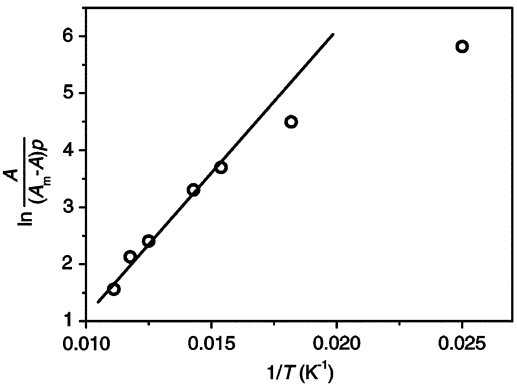

Fig. 8 Plot of the quantity $\ln\{A/[(A_M-A)p]\}$ *vs.* $(1/T)$ for the 4118–4112 cm^{-1} $Q_1(1)$ band of H_2 adsorbed on St-DVB.

simple benzene molecule can form H_2–C_6H_6 adducts in a perpendicular configuration where the H–H axis points toward the C_6H_6 plane in its centre, the interaction energy being 4.1 kJ mol^{-1}.[60] Despite the accuracy of the previous calculations, the consequences of the interaction on the vibrational properties of H_2 with respect to the free molecule has never been considered. In order to support the hypothesis of a specific interaction of H_2 with the St-DVB phenyl groups, we therefore decided to perform calculations aiming to predict the perturbation of the H_2 molecule in terms of the anharmonic vibrational frequency, *i.e.* a parameter directly comparable with the experimental evidences of Fig. 6. As a model for the H_2/St-DVB interaction we have assumed the already investigated H_2/H_6C_6 system, although roughly approximated. In fact, this simple cluster model does not take into consideration the effect of the cavity on the perturbation of encapsulated H_2, nor the presence of the lateral chains which can affect the electron density on the phenyl groups. In this latter respect, it has, for instance, been shown by Hübner *et al.*[57] that passing from benzene to toluene brings an increase in the BE of 0.47 kJ mol^{-1}. The calculations have been performed at the MP2 level, although it is known[57,60] that this method can overestimate the interaction energy of the H_2/C_6H_6 complex (about 20% with respect to CCSD(T)). All the parameters have been carefully corrected for the BSSE.

Three possible geometries of the H_2/C_6H_6 adducts have been considered: (i) an end-on arrangement with the H–H axis oriented perpendicularly to the ring plane (see Fig. 7); two side-on configurations where the H–H axis was parallel to the ring plane but aligned either (ii) along the direction defined by two opposite carbon atoms or (iii) perpendicularly to two opposite C–C bonds. As expected from the shape of the H_2 electrostatic potential, only the end-on complex resulted to be a minimum in agreement with previous calculations.[57] The results for this complex are summarized in Table 2 and in Fig. 7. The BSSE corrected binding energy (4.2 kJ mol^{-1}) is in good agreement with literature data.[57,60]

It is worth noting the very good agreement between the shift of the ν(HH) stretching frequency for the H_2–C_6H_6 adduct as obtained from the calculations (-33 cm^{-1}) and the experimental value for the H_2/St-DVB interaction (-35 cm^{-1} for the $Q_1(0)$ band: see Table 1). This reinforces the assignment of the spectra of Fig. 6 to the specific interaction of H_2 with the aromatic part (phenyl rings) of the polymer. Following the interaction, the H–H bond is polarized and weakened, accounting for the infrared activation of the ν(H–H) mode and the downward shift.

Spectroscopic evaluation of the H_2/St-DVB adsorption enthalpy

Collections of spectra like series 1–7 in Fig. 6a form the basis for the estimation of the molecule/surface interaction energy following the VTIR (variable temperature infrared) spectroscopic method,[7,8] which has already been successfully utilized for the weak adsorption of H_2 and other small molecules on a variety of materials.[7,8,20,38,39] Following the VTIR method, the adsorption enthalpy can be evaluated (in the Langmuir approximation) from the slope of the linear plot of $\ln\{A/[(A_M - A)p]\}$ *vs.* $(1/T)$, where $A \equiv A(T)$ is the intensity of an IR manifestation of the adsorbed species as a function of the temperature T, A_M is the intensity of the same manifestation corresponding to the complete (1 : 1) filling of the adsorbing sites and p is the equilibrium gas pressure.

By assuming for A_M the intensity of the $Q_1(1)$ band measured at 14 K and for $A(T)$ that of the same band measured at temperatures variable in the 95–14 K range, the plot reported in Fig. 8 is obtained for the H_2/St-DVB system. We can observe that the plot is fairly linear as far as the points corresponding to lower H_2 loadings are concerned, allowing

Table 2 Computed features of the H_2/C_6H_6 adduct as obtained by a BSSE-potential energy scan at the MP2/aug-cc-pVDZ level

	r^c/Å	Δd_{H-H}/Å	BE/kJ mol^{-1}	BE^c/kJ mol^{-1}	$\Delta\nu_{anharm}$/cm^{-1}
H_2/C_6H_6[a]	3.1745	0.0021	7.73	4.22	−33
H_2/C_6H_6[b]	2.9505	0.0019	8.40	3.71	−28

[a] BSSE-corrected geometry of interaction (see text). [b] BSSE-uncorrected geometries of interaction, that is by freely relaxing the geometry. [c] r: distance between the H_2 and C_6H_6 centers of mass; Δd_{H-H}: change of the H–H bond length upon complexation; BE: binding energy; BE^c: BSSE-corrected binding energy; $\Delta\nu_{anharm}$: shift of the H–H anharmonic frequency of adsorbed H_2 with respect to the free molecule. Calculated parameters for free H_2: d_{H-H} = 0.75493 Å, ν(H–H) = 4249.4 cm^{-1}.

to estimate adsorption enthalpy changes of the order of *ca.* 4 kJ mol^{-1}. This experimental value is in good agreement with present (Table 2) and previous[57,58,60] calculations for the H_2–benzene interaction, but lower than the 6.6 kJ mol^{-1} mean value reported by Germain *et al.* for the H_2 adsorption on nanoporous HCPs[31] (which, on the contrary, appears slightly overestimated in respect to the theoretical predictions).

Also evident in Fig. 8 is the progressive divergence from the linearity of the experimental points obtained at the lowest temperatures (*i.e.* at the highest H_2 coverages). This behavior resembles the rapid decrease of the heat of adsorption with saturation of the surface observed by Germain *et al.* on nanoporous HCPs[31] and could find its origin in the structural heterogeneity of the adsorbent (which indeed has a quite a broad pore-size distribution, as demonstrated in Fig. 2). Progressive filling of pores of increasing dimensions, and hence heterogeneous from an energetic point of view, is also the possible origin of the shift (12 cm^{-1}) of the ν(HH) frequency with coverage evident in Fig. 6b. As the shift can dramatically influence the extinction coefficient of ν(HH) mode, it follows that the intensity of the $Q_1(1)$ band could become more and more underestimated as the temperature decreases (*i.e.* as the ν(HH) band moves toward the gas phase frequency). It is then evident that the enthalpy change measured by the VTIR method for H_2/St-DVB must be considered as a mean value. In principle, the intensity of the $Q_1(1)$ band could be corrected by considering the extinction coefficient decrement. However, in this way the initial heat of adsorption is not much affected.

As a final comment, we outline that if reference is made to literature data concerning the $\Delta\tilde{\nu}$(HH)/binding energy relationship established for the interaction of molecular hydrogen with surface or isolated cationic sites,[20,61] the shift of the H–H stretching mode observed here (*ca.* 40 cm^{-1}) appears surprisingly large compared to the low experimental or calculated adsorption energy (*ca.* 4 kJ mol^{-1}). The difference is, on the contrary, conceivable with the theoretical expectations for the interaction of H_2 with negatively charged centres.[62] This further reinforces the view that the spectra of Fig. 6 are due to dihydrogen species interacting with the electron-rich part (phenyl groups) of the polymeric structure.

Conclusions

Microporous St-DVB [poly(styrene-*co*-divinylbenzene) polymer] characterized by a surface area of 920 m^2 g^{-1} reversibly adsorbs up to *ca.* 1.3 H_2 mass% at 1 bar and 1.8 H_2 mass% at 10 bar. The adsorption process primarily involves the specific interaction of the H_2 molecule with the electron-rich part of the polymer (phenyl rings), which results in the IR activation of the H–H stretching mode and the downward shift (37–45 cm^{-1}) of the H–H stretching frequency with respect to the gas phase. The H_2/phenyl ring interaction energy has been directly evaluated from the spectra and results *ca.* 4 kJ mol^{-1}. The low interaction energy accounts for the permanence of some rotational degree of freedom of the adsorbed molecules as revealed by the IR spectra. *Ab initio* calculations predict an end-on configuration of the H_2/phenyl adducts with H–H axis perpendicular to the aromatic ring in its centre. Changes in the *ortho*-/*para*-H_2 composition of the adsorbed phase with contact time at 14 K are also evidenced.

Acknowledgements

Financial support by *Regione Piemonte* in the frame of the research project "Innovative materials for hydrogen storage" is gratefully acknowledged.

References

1 L. Schlapbach and A. Züttel, *Nature*, 2001, **414**, 353.
2 A. Züttel, *Naturwiss.*, 2004, **91**, 157.
3 A. M. Seayad and D. M. Antonelli, *Adv. Mater.*, 2004, **16**, 765.
4 K. M. Thomas, *Catal. Today*, 2007, **120**, 389.
5 S. K. Bhatia and A. L. Myers, *Langmuir*, 2006, **22**, 1688.
6 G. Spoto, E. Gribov, S. Bordiga, C. Lamberti, G. Ricchiardi, D. Scarano and A. Zecchina, *Chem. Commun.*, 2004, 2768.
7 E. Garrone and C. Otero Areán, *Chem. Soc. Rev.*, 2005, **34**, 846.
8 C. Otero Areán, D. Nachtigallova, P. Nachtigall, E. Garrone and M. Delgado Rodriguez, *Phys. Chem. Chem. Phys.*, 2007, DOI: 10.1039/b615535a.
9 G. Spoto, S. Bordiga, A. Zecchina, D. Cocina, E. N. Gribov, L. Regli, E. Groppo and C. Lamberti, *Catal. Today*, 2006, **113**, 65.
10 M. G. Nijkamp, J. E. M. J. Raaymakers, A. J. van Dillen and K. P. de Jong, *Appl. Phys. A*, 2001, **72**, 619.
11 H. G. Schimmel, G. J. Kearley, M. G. Nijkamp, C. T. Visser, K. P. de Jong and F. M. Mulder, *Chem.–Eur. J.*, 2003, **9**, 4764.
12 M. Hirscher and M. Becher, *J. Nanosci. Nanotechnol.*, 2003, **3**, 3.
13 L. Zhou, Y. Zhou and Y. Sun, *Int. J. Hydrogen Energy*, 2006, **31**, 259.
14 B. Panella, M. Hirscher and S. Roth, *Carbon*, 2005, **43**, 2209.
15 A. Ansón, J. Jagiello, J. B. Parra, M. L. Sanjuán, A. M. Benito, W. K. Maser and M. T. Martínez, *J. Phys. Chem. B*, 2004, **108**, 15820.
16 T. Heine, L. Zhechkov and G. Seifert, *Phys. Chem. Chem. Phys.*, 2004, **6**, 980.
17 J. Weitkamp, M. Fritz and S. Ernst, *Int. J. Hydrogen Energy*, 1995, **20**, 967.
18 J. G. Vitillo, G. Ricchiardi, G. Spoto and A. Zecchina, *Phys. Chem. Chem. Phys.*, 2005, **7**, 1.
19 A. Zecchina, S. Bordiga, J. G. Vitillo, G. Ricchiardi, C. Lamberti, G. Spoto, M. Bjørgen and K. P. Lillerud, *J. Am. Chem. Soc.*, 2005, **127**, 6361.
20 A. Zecchina, G. Spoto and S. Bordiga, *Phys. Chem. Chem. Phys.*, 2005, **7**, 1627.
21 N. L. Rosi, J. Eckert, M. Eddaoudi, D. T. Vodak, J. Kim, M. O'Keeffe and O. M. Yaghi, *Science*, 2003, **300**, 1127.
22 G. Ferey, M. Latroche, C. Serre, F. Millange, T. Loiseau and A. Percheron-Guegan, *Chem. Commun.*, 2003, 2976.
23 L. Pan, M. B. Sander, X. Huang, J. Li, M. Smith, E. Bittner, B. Bockrath and J. K. Johnson, *J. Am. Chem. Soc.*, 2004, **126**, 1308.
24 J. L. C. Rowsell and O. M. Yaghi, *Angew. Chem., Int. Ed.*, 2005, **44**, 4670.
25 S. Bordiga, J. G. Vitillo, G. Ricchiardi, L. Regli, D. Cocina, A. Zecchina, B. Arstad, M. Bjørgen, J. Hafizovic and K. P. Lillerud, *J. Phys. Chem. B*, 2005, **109**, 18237.
26 N. W. O. Banglin Chen, Andrew R. Millward, Damacio S. Contreras and Omar M. Yaghi, *Angew. Chem., Int. Ed.*, 2005, **44**, 4745.
27 B. N. McKeown and P. M. Budd, *Chem. Soc. Rev.*, 2005, **35**, 675.
28 B. N. McKeown, B. Gahnem, K. J. Msayib, P. M. Budd, C. E. Tattershall, K. Mahmood, S. Tan, D. Book, H. W. Langmi and A. Walton, *Angew. Chem., Int. Ed.*, 2006, **45**, 1804.
29 P. M. Budd, A. Butler, J. Selbie, K. Mahmood, B. N. McKeown, B. Gahnem, K. J. Msayib, D. Book and A. Walton, *Phys. Chem. Chem. Phys.*, 2007, DOI: 10.1039/b618053a.
30 J.-Y. Lee, C. D. Wood, D. Bradshaw, M. J. Rosseinsky and A. I. Cooper, *Chem. Commun.*, 2006, 2670.
31 J. Germain, J. Hradil, J. M. J. Fréchet and F. Svec, *Chem. Mater.*, 2006, **18**, 4430.

32 X. Lin, J. Jia, X. Zhao, K. M. Thomas, A. J. Blake, G. S. Walker, N. R. Champness, P. Hubberstey and M. Schröder, *Angew. Chem., Int. Ed.*, 2006, **45**, 7358.
33 N. Texier-Mandoki, J. Dentzer, T. Piquero, S. Saadallah, P. David and C. Vix-Guterl, *Carbon*, 2004, **42**, 2735.
34 V. A. Davankov and M. P. Tsyurupa, *React. Polym.*, 1990, **13**, 27.
35 J.-H. Ahn, J.-E. Jang, C.-G. Oh, S.-K. Ihm, J. Cortez and D. C. Sherrington, *Macromolecules*, 2006, **39**, 627.
36 B. N. McKeown, P. M. Budd, K. J. Msayib, B. Gahnem, H. J. Kingston, C. E. Tattershall, S. Makhseed, K. J. Reynolds and D. Fritsch, *Chem.–Eur. J.*, 2005, **11**, 2160.
37 P. M. Budd, B. N. McKeown and D. Fritsch, *J. Mater. Chem.*, 2005, **15**, 1977.
38 N. E. Gribov, D. Cocina, G. Spoto, S. Bordiga, G. Ricchiardi and A. Zecchina, *Phys. Chem. Chem. Phys.*, 2006, **8**, 1186.
39 E. N. Gribov, S. Bertarione, D. Scarano, C. Lamberti, G. Spoto and A. Zecchina, *J. Phys. Chem. B*, 2004, **108**, 16174.
40 G. Spoto, E. Gribov, G. Ricchiardi, A. Damin, D. Scarano, S. Bordiga, C. Lamberti and A. Zecchina, *Prog. Surf. Sci.*, 2004, **76**, 71.
41 C. Møller and M. S. Plesset, *Phys. Rev.*, 1934, **46**, 618.
42 M. J. Frisch, G. W. Trucks, H. B. Schlegel, G. E. Scuseria, M. A. Robb, J. R. Cheeseman, J. Montgomery, J. A., T. Vreven, K. N. Kudin, J. C. Burant, J. M. Millam, S. S. Iyengar, J. Tomasi, V. Barone, B. Mennucci, M. Cossi, G. Scalmani, N. Rega, G. A. Petersson, H. Nakatsuji, M. Hada, M. Ehara, K. Toyota, R. Fukuda, J. Hasegawa, M. Ishida, T. Nakajima, Y. Honda, O. Kitao, H. Nakai, M. Klene, X. Li, J. E. Knox, H. P. Hratchian, J. B. Cross, V. Bakken, C. Adamo, J. Jaramillo, R. Gomperts, R. E. Stratmann, O. Yazyev, A. J. Austin, R. Cammi, C. Pomelli, J. W. Ochterski, P. Y. Ayala, K. Morokuma, G. A. Voth, P. Salvador, J. J. Dannenberg, V. G. Zakrzewski, S. Dapprich, A. D. Daniels, M. C. Strain, O. Farkas, D. K. Malick, A. D. Rabuck, K. Raghavachari, J. B. Foresman, J. V. Ortiz, Q. Cui, A. G. Baboul, S. Clifford, J. Cioslowski, B. B. Stefanov, G. Liu, A. Liashenko, P. Piskorz, I. Komaromi, R. L. Martin, D. J. Fox, T. Keith, M. A. Al-Laham, C. Y. Peng, A. Nanayakkara, M. Challacombe, P. M. W. Gill, B. Johnson, W. Chen, M. W. Wong, C. Gonzalez and J. A. Pople, *GAUSSIAN 03*, Gaussian Inc., Wallingford, CT, 2004.
43 R. A. Kendall, T. H. Dunning and R. J. Harrison, *J. Chem. Phys.*, 1992, **96**, 6796.
44 K. A. Peterson, D. E. Woon and T. H. Dunning, *J. Chem. Phys.*, 1994, **100**, 7410.
45 S. F. Boys and F. Bernardi, *Mol. Phys.*, 1970, **19**, 553.
46 B. Lindberg, *J. Chem. Phys.*, 1988, **88**, 3805.
47 P. Ugliengo, *ANHARM-A program to solve monodimensional nuclear Schrödinger equation*, unpublished, 1989.
48 S. J. Gregg and K. S. W. Sing, *Adsorption, surface area and porosity*, Academic Press Inc., London, 2nd edn, 1982.
49 M. Jaroniec, M. Kruk, J. P. Olivier and S. Koch, *Stud. Surf. Sci. Catal.*, 2000, **128**, 71.
50 G. F. R. S. Herzberg, *Molecular spectra and molecular structure I. Diatomic molecules*, D. Van Nostrand Company Inc., New York, 1950.
51 B. P. Stoicheff, *Can. J. Phys.*, 1957, **35**, 730.
52 S. S. Bhatnagar, E. J. Allin and H. L. Welsh, *Can. J. Phys.*, 1962, **40**, 9.
53 Y. Y. Milenko and R. M. Sibileva, *J. Low Temp. Phys.*, 1997, **107**, 77.
54 B. F. Minaev and H. Ågren, *J. Phys. Chem.*, 1995, **99**, 8936.
55 H. P. Gush, W. F. J. Hare, E. J. Allin and H. L. Welsh, *Can. J. Phys.*, 1960, **38**, 176.
56 V. B. Kazansky, *J. Mol. Catal. A*, 1999, **141**, 83.
57 O. Hübner, A. Glöss, M. Fichtner and W. Klopper, *J. Phys. Chem. A*, 2004, **108**, 3019.
58 S. Hamel and M. Côté, *J. Chem. Phys.*, 2004, **121**, 12618.
59 Y. Okamoto and Y. Miyamoto, *J. Phys.Chem. B*, 2001, **105**, 3470.
60 A. Ferre-Vilaplana, *J. Chem. Phys.*, 2005, **122**, 104709.
61 J. G. Vitillo, A. Damin, A. Zecchina and G. Ricchiardi, *J. Chem. Phys.*, 2005, **122**, 114311.
62 J. G. Vitillo, A. Damin, A. Zecchina and G. Ricchiardi, *J. Chem. Phys.*, 2006, **124**, 224308.